JOURNAL OF COMPUTATIONAL PHYSICS 2, 178-196 (1967)

Difference Methods for the Inviscid and Viscous Equations of a Compressible Gas[1]

EPHRAIM L. RUBIN[2]

Polytechnic Institute of Brooklyn, Graduate Center,

Farmingdale, New York 11735

AND

SAMUEL Z. BURSTEIN[3]

Courant Institute of Mathematical Sciences, New York University, New York 10012

ABSTRACT

In this paper we examine several second-order accurate schemes for the solution of one-dimensional flows containing discontinuities.

Two problems of shock interactions have been considered, and two generalizations of these schemes have been used for the solution of the Navier-Stokes equations.

I. INTRODUCTION

In this paper we examine a series of one-dimensional flows containing discontinuities. Unlike characteristic methods the discontinuities are not considered to be internal moving boundaries. The description of the motion of the discontinuity is obtained from the solution of the differential equations. Hence the methods used to integrate the differential equations yield weak solutions (solutions which need not be differentiable) in the space-time domain. Several second-order accurate schemes are tested and compared. These second-order methods are characterized by small truncation error and confinement of the shock transition

[1] This research was sponsored in part by the Office of Naval Research under Contract No. Nonr 839 (34), Project No. NR 061–135, and by the Atomic Energy Commission under Contract No. AT(30–1)–1480. The authors would like to thank Mrs. Eleanor Kolchin for writing the eigenvalue code and for her excellent job of programming.

[2] Associate Professor, Dept. of Aerospace Engineering and Applied Mechanics.

[3] Assistant Professor.

to a narrow region of two or three mesh points. First-order schemes may require several times the number of mesh points to describe the same transition.

Two problems of shock interactions have been considered. They include the overtaking of one shock wave by another and the head-on collision of two shock waves.

Finally, two generalizations of these schemes have been examined and used for the solution of the Navier-Stokes equations.

II. Differential Equations

The equations of hydrodynamics may be written in vector form:

$$w_t = f_x \tag{1}$$

where w is a vector function of x and t

$$w = \begin{pmatrix} \rho \\ m \\ E \end{pmatrix}, \tag{2}$$

and f is a given nonlinear vector function of w, i.e.,

$$f = \begin{pmatrix} -m \\ -\left(\frac{m^2}{\rho} + p\right) \\ -\frac{m}{\rho}(p + E) \end{pmatrix}. \tag{3}$$

The mass ρ, momentum m, and total energy E are all per unit volume. The total energy is written as the sum of the kinetic energy $m^2/2\rho$ and the internal energy ρe.

$$E = m^2/2\rho + \rho e$$

and the pressure is given by the equation of state,

$$p = \rho(\gamma - 1)e = (\gamma - 1)(E - m^2/2\rho), \tag{4}$$

where γ is the ratio of specific heats.

III. Difference Equations

The class of methods to be discussed are defined on the half plane $t \geqslant 0$, $-\infty < x < \infty$, where $\{x_{\pm n} = \pm n\,\Delta x,\ t_i = i\Delta t;\ n, i = 0, 1, 2,...\}$ define the uniformly spaced net points of the lattice. We call $w_n{}^i = w(n\Delta x, t)$ the mesh function which is defined on this lattice and which constitutes an approximation to the

solution of the differential equation (1). We will consider difference approximations of the form

$$\delta_t w = \delta_x f,$$

where δ_t, δ_x are suitable difference operators which approximate the partial derivative operators of Eq. (1). In the discussion that follows, the form of δ_t and δ_x for several difference schemes will be given.

The Lax-Wendroff scheme is based on the Taylor series expansion of the vector function $w(x, t + \Delta t)$ so as to include the second-order term w_{tt}. This term is expressed in terms of space differences using Eq. (1); i.e., w_{tt} may be written as $w_{tt} = (f_x)_t = (f_t)_x = (Aw_t)_x = (Af_x)_x$, where A is the matrix whose determinant is the Jacobian of $f(w)$ with respect to w. The value of w at time $t + \Delta t$ and point n on the mesh may then be given by

$$w_n^{t+\Delta t} = w_n{}^t + \frac{\Delta t}{2\Delta x}[f_{n+1}^t - f_{n-1}^t] + \frac{1}{4}\left(\frac{\Delta t}{\Delta x}\right)^2 [(A_{n+1} + A_n)(f_{n+1}^t - f_n{}^t) - (A_n + A_{n-1})(f_n{}^t - f_{n-1}^t)]. \tag{5}$$

A two-step method obtained by Richtmyer [1] is referred to as a two-step Lax-Wendroff scheme. The values at the intermediate points are computed at a time $t + \Delta t$ using a first-order scheme, and then a second-order scheme (leap frog) is used to compute the value at time $t + 2\Delta t$. The overall scheme has second order accuracy. This paper describes several variations of Richtmyer's two-step method for two independent variables. For three independent variables, the reader is referred to one of the author's recent paper [2]. It is possible to write Richtmyer's scheme so as to require only one-half the mesh spacing

$$w_{n+\frac{1}{2}}^{t+\Delta t/2} = \frac{w_{n+1}^t + w_n{}^t}{2} + \frac{\Delta t}{2\Delta x}[f_{n+1}^t - f_n{}^t] \tag{6a}$$

$$w_n^{t+\Delta t} = w_n{}^t + \frac{\Delta t}{\Delta x}[f_{n+\frac{1}{2}}^{t+\Delta t/2} - f_{n-\frac{1}{2}}^{t+\Delta t/2}]. \tag{6b}$$

If, instead of computing the intermediate values at time $t + (\Delta t/2)$, we compute them at $t + \Delta t$ and then average the f differences at t and $t + \Delta t$ so that both the w and f values are centered at point $(n, t + \Delta t/2)$, the following difference approximation is obtained:

$$w_{n+\frac{1}{2}}^{t+\Delta t} = \frac{w_{n+1}^t + w_n{}^t}{2} + \frac{\Delta t}{\Delta x}[f_{n+1}^t - f_n{}^t] \tag{7a}$$

$$w_n^{t+\Delta t} = w_n{}^t + \frac{\Delta t}{2\Delta x}\left[\frac{f_{n+1}^t - f_{n-1}^t}{2} + f_{n+\frac{1}{2}}^{t+\Delta t} - f_{n-\frac{1}{2}}^{t+\Delta t}\right]. \tag{7b}$$

It should be noted that the linearized forms of systems (6) and (7) reduce to the Lax-Wendroff scheme, Eq. (5). We shall discuss this point later in the paper.

IV. Numerical Results to Several Test Problems

A comparison of the three methods was made by examining them at different values of $\lambda = \Delta t/\Delta x$. For $\lambda = .48$ CFL, i.e., 0.48 of the Courant-Friedrichs-Lewy stability condition, $\lambda \leqslant 1/|u| + a$, the results for all three schemes were essentially the same. In Fig. 1, the density vs distance plots are shown for the fiftieth time step. The shape of these curves remained unchanged at time step 200. Figure 2

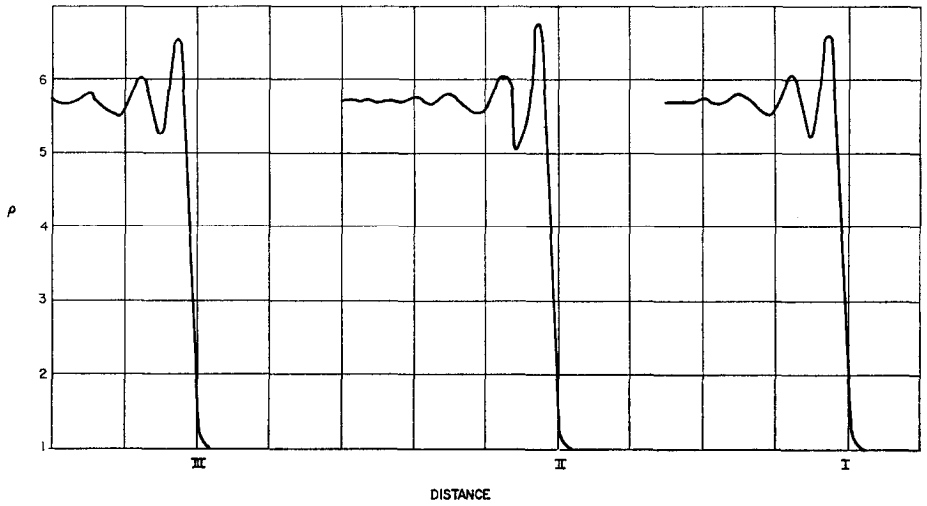

FIG. 1. Density vs distance at time step 50; $\Delta t/\Delta x = .48$ CFL.

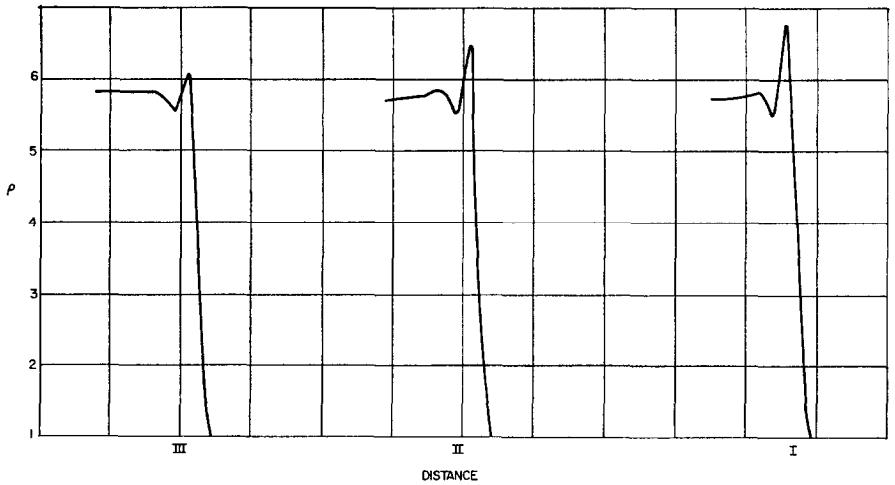

FIG. 2. Density vs distance at time step 50; $\Delta t/\Delta x = .79$ CFL.

shows the results for $\lambda = .79$ CFL and again they did not change with further integrations in time. The overshoot behind the shock for system (7) is seen to be smaller than it was for the previous value of λ and, in fact, the oscillation decreases as the stability limit is approached. It is apparent that the difference approximation given by Eq. (7) has the greatest damping for this problem since the overshoots obtained from the other two schemes are substantially larger.

All schemes become unstable at $\lambda = \text{CFL}$. Figures 3 and 4 show the results for

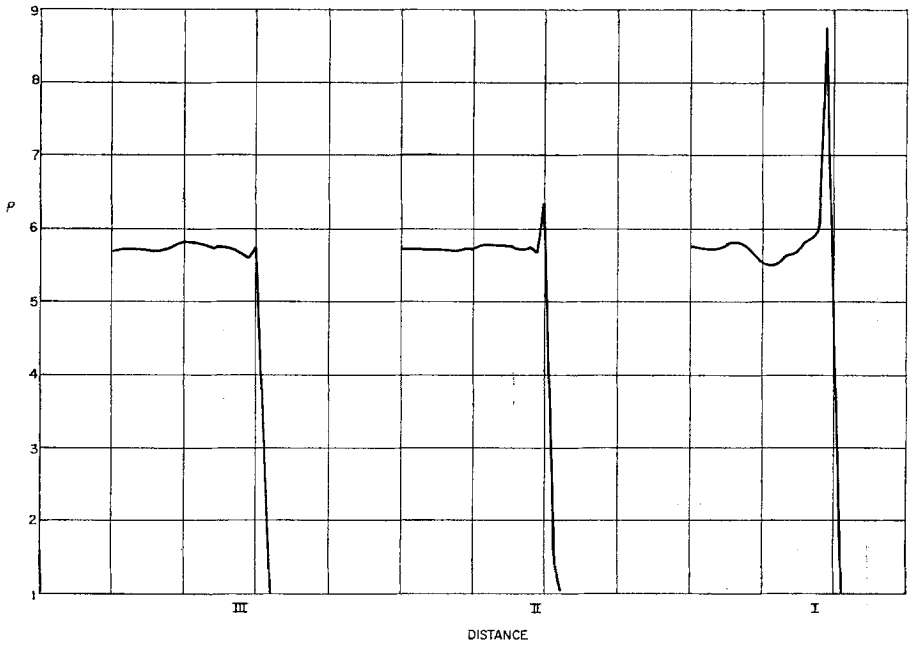

FIG. 3. Density vs distance at time step 50; $\Delta t/\Delta x = .98$ CFL.

$\lambda = .98$ CFL for 50 and 100 time steps, respectively. Difference approximation (7) is clearly the best and gives virtually no overshoot. The original Lax-Wendroff method, Eq. (5), does not improve as you approach the stability limit as opposed to system (6) which does. Based on numerical experiments of bore formation in the atmosphere [3], the Lax-Wendroff scheme in the shallow water equations also exhibits variable damping characteristics with increasing λ.

As an example of an interaction problem, we investigated the case of two equal strength shock waves undergoing a head-on collision. The problem is illustrated in Fig. 5. The initial conditions are for shocks of Mach number 10, each connecting two constant states. The pressure, density, and velocity were assigned the value of

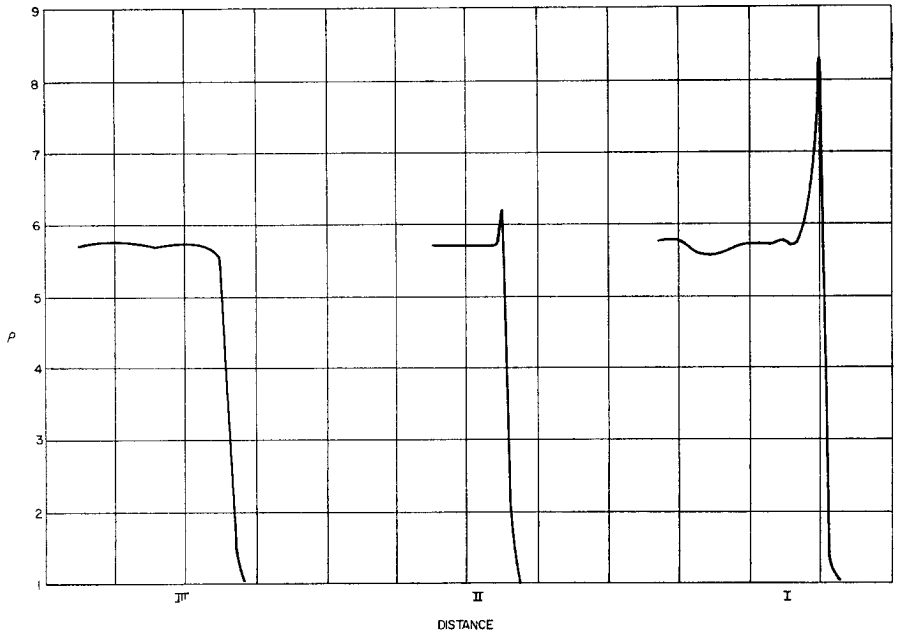

FIG. 4. Density vs distance at time step 100; $\Delta t/\Delta x = .98$ CFL.

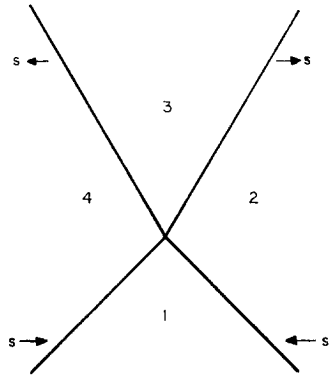

FIG. 5. Head-on collision of two equal shock waves.

unity in the undisturbed state. The shocks connected this states with two states labeled 2 and 4. The results (two receding shock waves) for the following initial conditions are shown in Fig. 6:

$$\rho_4 = 5.7142 \qquad \rho_2 = 5.7142$$
$$u_4 = 10.7615 \qquad u_2 = -8.7615$$
$$p_4 = 116.5 \qquad p_2 = 116.5$$
$$\gamma = 1.4 \qquad \gamma = 1.4$$

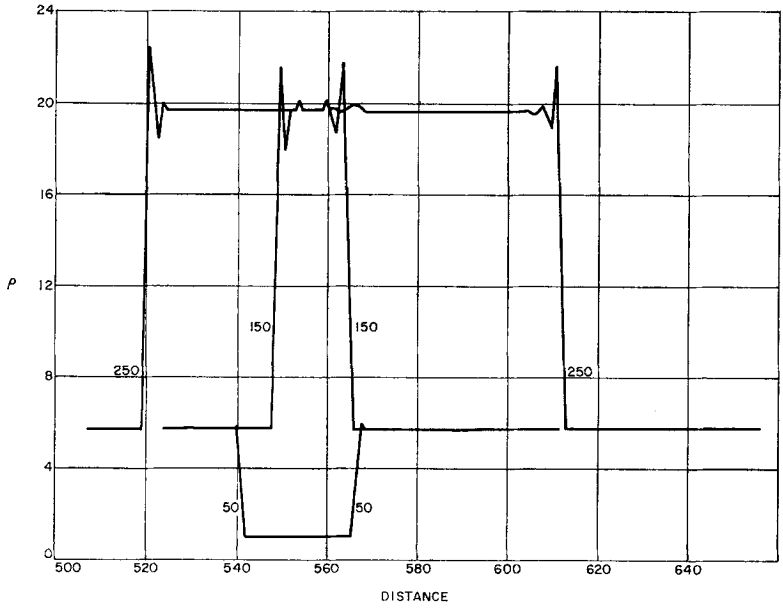

FIG. 6. Density vs distance for two colliding shocks; scheme 3; $\Delta t/\Delta x = .98$ CFL.

The calculation was carried out using system (7) with $\lambda = .98$ CFL. The other two methods gave similar results with larger density overshoots near the tail of the shocks. The theoretical pressure ratio across the shock may be calculated from the Rankine-Hugoniot relations which, under suitable algebraic manipulation, lead to the following expression:

$$\frac{p_3}{p_4} = \frac{2 + \tau - p_1/p_4}{1 + \tau(p_1/p_4)}, \qquad \tau = \frac{\gamma + 1}{\gamma - 1}.$$

The theoretical pressure ratio is 7.51 for $\gamma = 1.4$; the computed value was 7.69.

Another interesting problem that was used as a test of these methods was the overtaking of one shock wave by another. It is known that for $\gamma \leqslant \frac{5}{3}$, the fluid

after the interaction will contain a transmitted shock, a reflected rarefaction wave, and a contact surface which connects the two constant states (see von Neumann[4]). Plots for density and pressure vs distance are shown in Figs. 7 and 8 and were computed using the maximum allowable value of λ.

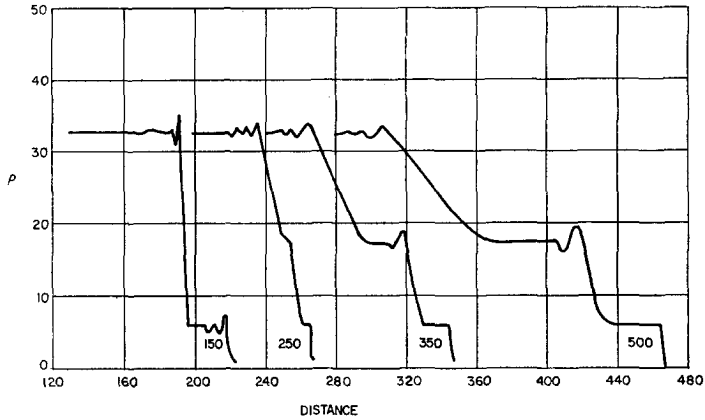

FIG. 7. Density vs distance for coalescing shocks.

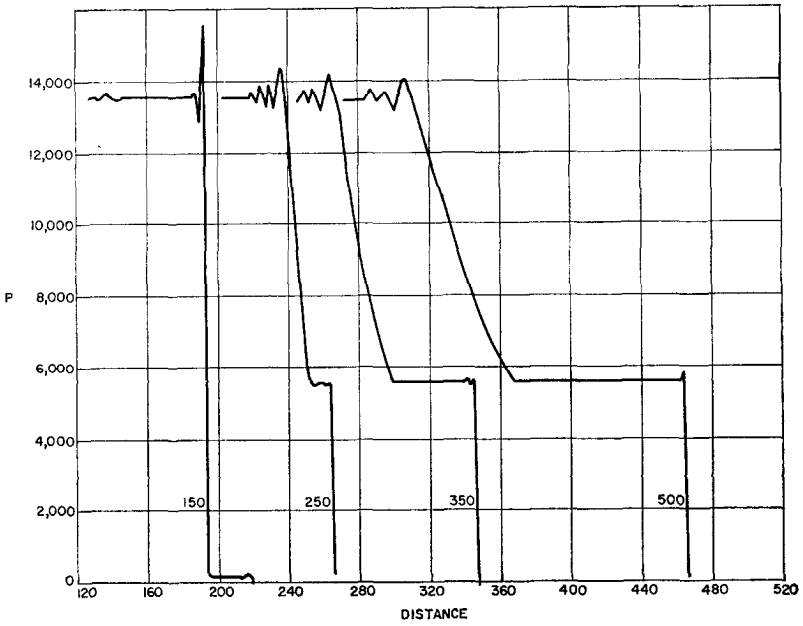

FIG. 8. Pressure vs distance for coalescing shocks.

V. Analysis of Viscosity for the Three Lax-Wendroff Schemes

In an effort to account theoretically for the difference in behavior of the three schemes, Eqs. (5–7), we examined the stability criteria for each of them. This requires a linearization of the equations, i.e., we write them in matrix form:

$$w_t = Aw_x$$

Here A is the Jacobian of the transformation and is now to be regarded as constant. This linearized partial differential equation is now differenced according to the rules specified by Eqs. (5–7). We next consider a solution of the form $w_n{}^t = \bar{w}(t)e^{ikx}$ and substitute it into the difference scheme. This leads to the quotient $[\bar{w}(t + \Delta t)]/[\bar{w}(t)]$, which is the growth factor for the amplitude of the kth harmonic for the time-interval Δt. We call G the amplification matrix for the particular difference scheme and for stability, the eigenvalues of G should be, in absolute value, less than or equal to one. For all three cases the amplification matrix becomes

$$G = I + i\lambda A \sin \xi + \lambda^2 A^2(\cos \xi - 1),$$

where I is the unit matrix and $\xi = k\Delta x$. Thus the stability criteria is the same for all three schemes; the reader is referred to a proof by Lax and Wendroff [5] on the stability of difference schemes whose amplification matrix is G.

The Lax–Wendroff scheme, Eq. (5), may be written correct to third order as

$$\begin{aligned}
&\frac{1}{\Delta t}\left[w(t + \Delta t, x) - w(t, x)\right] \\
&\quad = \frac{1}{\Delta x}\left\{f\left(t, x + \frac{\Delta x}{2}\right) - f\left(t, x - \frac{\Delta x}{2}\right)\right. \\
&\qquad + \left[f_t\left(t, x + \frac{\Delta x}{2}\right) - f_t\left(t, x - \frac{\Delta x}{2}\right)\right]\frac{\Delta t}{2} \\
&\qquad + \left[f_{tt}\left(t, x + \frac{\Delta x}{2}\right) - f_{tt}\left(t, x - \frac{\Delta x}{2}\right)\right]\frac{(\Delta t)^2}{6} \\
&\qquad \left. + \left[f_{ttt}\left(t, x + \frac{\Delta x}{2}\right) - f_{ttt}\left(t, x - \frac{\Delta x}{2}\right)\right]\frac{(\Delta t)^3}{24}\right\}.
\end{aligned}$$

Expanding the other two schemes in a similar way and writing:

$$f\left(t, x + \frac{\Delta x}{2}\right) - f\left(t, x - \frac{\Delta x}{2}\right) = \frac{f(t, x + \Delta x) - f(t, x - \Delta x)}{2},$$

it is apparent that to first-order schemes (5–7) are identical. One would expect the coefficient of the Δt term to be a measure of the viscosity, since it is this term which, if set equal to zero, with the higher order terms, gives rise to an uncon-

ditionally unstable scheme. The coefficient, however, is $\frac{1}{2}$ for all three schemes. The coefficients of the $(\Delta t)^2$ terms are $\frac{1}{6}$, $\frac{1}{8}$ and $\frac{1}{4}$ respectively and these relative magnitudes are maintained for higher powers of Δt. Thus, the nonlinear behavior of the particular difference scheme seems to play a strong role in the characteristic damping observed since the coefficient of the $(\Delta t)^2$ term, which may be thought of as an additional artificial viscosity, does not have a weight factor which correlates with the observed damping.

VI. Navier-Stokes Equations

In generalizing these schemes to solve the Navier–Stokes equations we did not consider the original Lax–Wendroff method since its generalization is considerably more complicated than the other two schemes, and the previous results did not seem to warrant it. The two schemes considered are given by systems (9) and (10).

We write the Navier–Stokes equations as

$$w_t = f_x + S, \tag{8}$$

where S is given by

$$S = \begin{pmatrix} 0 \\ \dfrac{\partial}{\partial x_i}\sigma_{i_1} \\ k\nabla^2 T + \dfrac{\partial}{\partial x_i}(u_j\sigma_{ij}) \end{pmatrix},$$

and

$$\sigma_{ij} = \mu\left(\frac{\partial u_i}{\partial x_j} + \frac{\partial u_j}{\partial x_i}\right) + \left(\mu' - \frac{2}{3}\mu\right)\frac{\partial u_k}{\partial x_k}\delta_{ij}.$$

Here, k is the thermal conductivity, μ the viscosity, and μ' is the second coefficient of viscosity, sometimes called the dilatational viscosity which we take to be zero. The equation of state is given by

$$p = \rho RT.$$

The equations are nondimensionalized in the usual way; i.e., we introduce a length L, velocity U, and density ρ_0. Momentum is nondimensionalized with respect to $\rho_0 U$ and energy with respect to $\rho_0 U^2$. The explicit form of the S vector is then

$$S = \begin{pmatrix} 0 \\ \dfrac{4}{3Re}\left(\dfrac{m}{\rho}\right)_{xx} \\ \dfrac{1}{Re}\left\{\dfrac{\gamma}{\mathrm{Pr}}\left[\dfrac{E}{\rho} - \dfrac{1}{2}\left(\dfrac{m}{\rho}\right)^2\right]_{xx} + \dfrac{4}{3}\left[\left(\dfrac{m}{\rho}\right)_x\right]^2 + \dfrac{4}{3}\dfrac{m}{\rho}\left(\dfrac{m}{\rho}\right)_{xx}\right\} \end{pmatrix},$$

where Re and Pr are the Reynolds and Prandtl numbers, respectively.

We now give the two schemes considered:

$$\bar{w}_{n+\frac{1}{2}}^{t+\Delta t/2} = \frac{w_{n+1}^t + w_n{}^t}{2} + \frac{\Delta t}{2\Delta x}[f_{n+1}^t - f_n{}^t] + \frac{\Delta t}{4}[S_{n+1}^t + S_n{}^t]$$

$$\bar{w}_n^{t+\Delta t/2} = \frac{w_{n+1}^t + w_{n-1}^t}{2} + \frac{\Delta t}{4\Delta x}[f_{n+1}^t - f_{n-1}^t] + \frac{\Delta t}{2} S_n{}^t \tag{9}$$

$$w_n^{t+\Delta t} = w_n{}^t + \frac{\Delta t}{\Delta x}[\bar{f}_{n+\frac{1}{2}}^{t+\Delta t/2} - \bar{f}_{n-\frac{1}{2}}^{t+\Delta t/2}] + \Delta t \bar{S}_n^{t+\Delta t/2},$$

where the bars signify intermediate values.

$$\bar{w}_{n+\frac{1}{2}}^{t+\Delta t} = \frac{w_{n+1}^t + w_n{}^t}{2} + \frac{\Delta t}{\Delta x}[f_{n+1}^t - f_n{}^t] + \frac{\Delta t}{2}[S_{n+1}^t + S_n{}^t]$$

$$\bar{w}_n^{t+\Delta t} = \frac{w_{n+1}^t + w_{n-1}^t}{2} + \frac{\Delta t}{2\Delta x}[f_{n+1}^t - f_{n-1}^t] + \Delta t S_n{}^t.$$

The preceding two equations are used for calculating the intermediate values for the second scheme. For the final value at point n at time $t + \Delta t$ we use

$$w_n^{t+\Delta t} = w_n{}^t + \frac{\Delta t}{2\Delta x}\left[\frac{f_{n+1}^t - f_{n-1}^t}{2} + \bar{f}_{n+\frac{1}{2}}^{t+\Delta t} - \bar{f}_{n-\frac{1}{2}}^{t+\Delta t}\right] + \frac{\Delta t}{2}[S_n{}^t + \bar{S}_n^{t+\Delta t}]. \tag{10}$$

System (9) is unstable; i.e., as the Reynolds number was decreased the densities became negative locally. In addition, the shock speed decreased with increasing viscosity, whereas it should be independent of viscosity.

Some results for system (10) are shown in Table I. With decreasing Reynolds number oscillations appear behind the shock. However, the dependence of the computed shock speed on the Reynolds number was much less than that of system (9).

The second order difference schemes that we have been considering center both the time and space differences. If one considers a parabolic equation such as the heat equation, $U_t = \sigma U_{xx}$, centering both time and space differences at the same space-time point results in a difference scheme that is always unstable. However, if one takes a forward difference in time and centers the space difference at time t, then the difference scheme is stable if $\sigma \Delta t/(\Delta x)^2 \leqslant \frac{1}{2}$.

The Navier–Stokes equations are a mixed hyperbolic parabolic system. Calculating the S vector at time t, rather than at time $t + \Delta t/2$, represents a centering of the dissipation term at time t. To see if such a change really is a stabilizing factor,

TABLE I

SYSTEM (10); DENSITY FOR VARIOUS REYNOLDS NUMBERS

$Re = 450$	$Re = 4$	$Re = 1$	$Re = .6$
5.697	5.771	6.016	6.227
5.688	5.755	5.962	6.048
5.691	5.753	5.873	5.855
5.713	5.761	5.810	5.778
5.755	6.776	5.828	5.931
5.788	5.812	5.973	6.330
5.790	5.857	6.233	6.881
5.783	5.903	6.540	7.454
5.770	5.964	6.841	7.882
5.740	6.021	7.064	8.143
5.722	6.050	7.173	8.381
5.726	6.076	7.244	8.138
5.711	6.084	7.303	3.993
5.671	6.082	5.409	1.108
5.604	6.044	1.392	1.008
5.714	4.308	1.009	1.000
2.911	1.112	1.000	1.000
1.006	1.001	1.000	1.000
1.000	1.000	1.000	1.000
1.000	1.000	1.000	1.000

we examined the eigenvalues of the amplification matrix corresponding to system (10) with the final step given as

$$w_n^{t+\Delta t} = w_n{}^t + \frac{\Delta t}{2\Delta x}\left[\frac{f_{n+1}^t - f_{n-1}^t}{2} + f_{n+\frac{1}{2}}^{t+\Delta t} - f_{n-\frac{1}{2}}^{t+\Delta t}\right] + \Delta t S_n{}^t. \tag{11}$$

We first rewrote the S vector in the following way:

$$S = \begin{pmatrix} 0 \\ \dfrac{4}{3Re}\left(\dfrac{m}{\rho}\right)_x \\ \dfrac{1}{Re}\left\{\dfrac{\gamma}{\Pr}\left[\dfrac{E}{\rho} - \dfrac{1}{2}\left(\dfrac{m}{\rho}\right)^2\right]_x + \dfrac{4}{3}\dfrac{\Pr}{\gamma}\left[\dfrac{m}{\rho}\left(\dfrac{m}{\rho}\right)_x\right]\right\} \end{pmatrix}_x = S'_x.$$

Then, in matrix notation Eq. (8) becomes $w_t = (A + C)w_x + Bw_{xx}$, where A, B, and C are regarded as constant matrices for purposes of the stability investigation.

They are given explicitly as follows:

$$A = \frac{\partial f}{\partial w} = \begin{pmatrix} 0 & -1 & 0 \\ -\dfrac{(\gamma-3)m^2}{2\rho^2} & (\gamma-3)\dfrac{m}{\rho} & -(\gamma-1) \\ \dfrac{\gamma E m}{\rho^2} - \dfrac{(\gamma-1)m^3}{\rho^3} & -\dfrac{\gamma E}{\rho} + \dfrac{3(\gamma-1)m^2}{2\rho^2} & -\dfrac{\gamma m}{\rho} \end{pmatrix},$$

$$B = \frac{\partial S}{\partial w_x} = \begin{pmatrix} 0 & 0 & 0 \\ -\dfrac{4}{3Re}\dfrac{m}{\rho^2} & \dfrac{4}{3Re\rho} & 0 \\ \dfrac{1}{Re}\left\{\dfrac{\gamma}{\mathrm{Pr}}\left[-\dfrac{E}{\rho^2}+\dfrac{m^2}{\rho^3}\right]-\dfrac{4}{3}\dfrac{m^2}{\rho^3}\right\} & \dfrac{1}{Re}\left\{-\dfrac{\gamma m}{\mathrm{Pr}\rho^2}+\dfrac{4}{3}\dfrac{m}{\rho^2}\right\} & \dfrac{1}{Re}\dfrac{\gamma}{\mathrm{Pr}\rho} \end{pmatrix},$$

$C = \partial S/\partial w$, where the elements C_{ij} are given by

$$C_{11} = C_{12} = C_{13} = C_{22} = C_{23} = 0,$$

$$C_{21} = -\frac{4}{3Re}\frac{m_x}{\rho^2} + \frac{8}{3Re}\frac{m}{\rho^3}\rho_x,$$

$$C_{31} = \frac{1}{Re}\left\{\frac{\gamma}{\mathrm{Pr}}\left[-\frac{E_x}{\rho^2}+\frac{2E\rho_x}{\rho^3}+\frac{2mm_x}{\rho^3}-\frac{3m^2\rho_x}{\rho^4}\right]+\frac{4}{3}\left[-\frac{2mm_x}{\rho^3}+\frac{3m^2}{\rho^4}\rho_x\right]\right\},$$

$$C_{32} = \frac{1}{Re}\left\{\frac{\gamma}{\mathrm{Pr}}\left[-\frac{m_x}{\rho^2}+\frac{2m\rho_x}{\rho^3}\right]+\frac{4}{3}\left[\frac{m_x}{\rho^2}-\frac{2m}{\rho^3}\rho_x\right]\right\},$$

$$C_{33} = \frac{1}{Re}\left\{-\frac{\gamma}{\mathrm{Pr}}\frac{\rho_x}{\rho^2}\right\}.$$

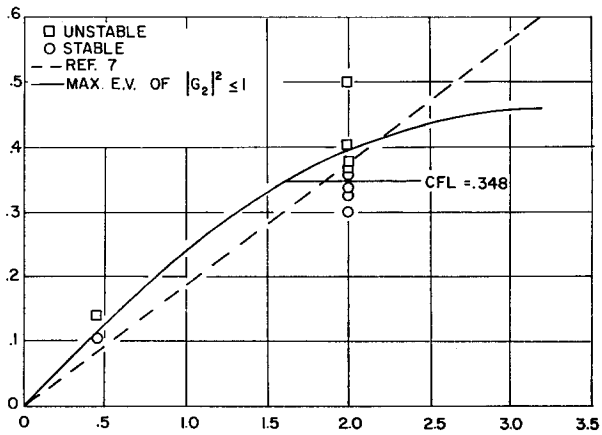

FIG. 9. Maximum eigenvalue of G_2 vs R_e.

Note, however, that the elements of matrix C are homogeneous in the first differential of the dependent variables. Then for smoothly varying solutions, only the elements of A need be considered for the coefficient of w_x. The linearized form that we consider is

$$w_t = Aw_x + Bw_{xx}.$$

We call G_1 the amplification matrix for system (10); G_2 is the amplification matrix for scheme (11). It then follows by the usual arguments that

$$G_1 = I + \lambda^2(\cos\xi - 1)A^2 + \epsilon(1 - \cos\xi)B + \epsilon^2(4\cos^2\xi - 8\cos\xi + 4)B^2 + i\{\lambda\sin\xi)A + \lambda\epsilon(\sin\xi\cos\xi - \sin\xi)AB\},$$

and

$$G_2 = I + \lambda^2(\cos\xi - 1)A^2 + 2\epsilon(\cos\xi - 1)B + i\{\lambda(\sin\xi)A + \lambda\epsilon(\sin\xi\cos\xi - \sin\xi)AB\},$$

I is the unit matrix $\xi = k\Delta x$, and $\epsilon = \Delta t/(\Delta x)^2$.

To calculate the complex eigenvalues of the matrices G_1 and G_2 we expanded the determinants and used Cardan's solution of the cubic equations. We chose the Courant-Friedrichs-Lewy condition for a first estimate. The eigenvalues of G_1 and G_2 for values of ξ evenly spaced from zero to π were computed. If the absolute value of the eigenvalues was greater than one, Δt was reduced and the calculation repeated.

We found, for $\Delta t > 0$, that the absolute values of the eigenvalues of G_1 were always greater than one. However, the value of Δt for which the magnitude of the eigenvalues of G_2 were less than one is bounded away from zero. All calculations reported in this paper were performed with scheme (11), which was first used by Thommen [6].

In Fig. 9, the absolute value of the maximum eigenvalue of G_2 is plotted as a function of Reynolds number. The stability condition of Gary [7] is also plotted for comparison. The CFL condition requires $\Delta t \leqslant .348$. Several computed runs for system (11) were carried out to 400 cycles for two values of the Reynolds number. The stable runs are indicated by circles, unstable runs by squares. It is seen that stability is assured if it is chosen such that

$$\Delta t \leqslant \min\left[\frac{\Delta x}{u + a}, \Delta t_v\right]$$

where Δt_v is that value of $\lambda\Delta x$ which assures the maximum absolute eigenvalue of G_2 is less than unity.

The actual calculations were performed with initial conditions corresponding to a right moving shock travelling at a Mach number of 1.6 with respect to the

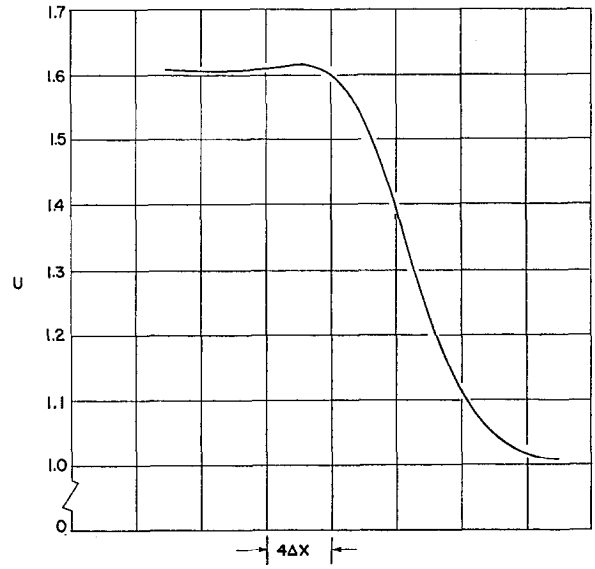

FIG. 10. Velocity distribution for Pr = .75, $Re = 4.5$, $M = 1.6$, $\gamma = 1.4$.

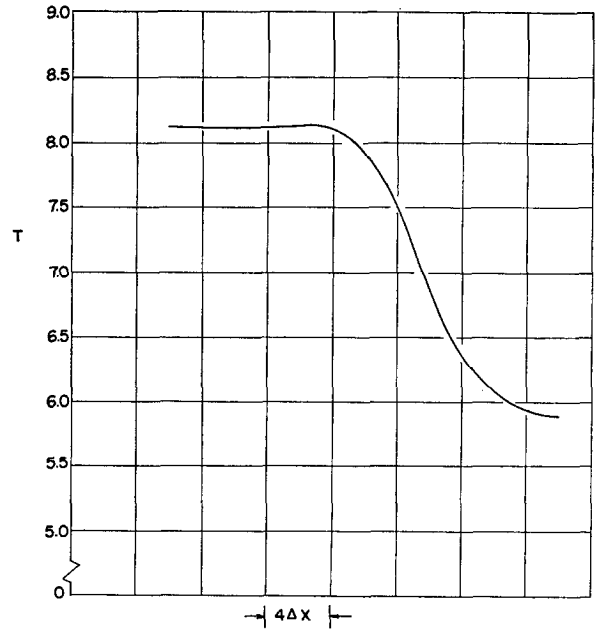

FIG. 11. Temperature distribution for Pr = .75, $Re = 4.5$, $M = 1.6$, $\gamma = 1.4$.

undisturbed fluid. The Rankine-Hugoniot relations were used to compute the state behind the shock.

To check the convergence of system (10) with these initial conditions we ran three cases each for a real time of 20. λ was taken to be successively .2/1, .05/.20, and .0125/.125 and the number of integration cycles to be 100, 400, and 1600, respectively.

Corresponding points for the last two runs agreed to within 1% and all subsequent calculations were performed with $\lambda = .05/.20$.

We now proceeded to investigate the change in properties through the shock for different Reynolds and Prandtl number. The results are in qualitative agreement with the steady state calculations of Morduchow and Libby [8], to whose paper the reader is referred for other references on the subject. Since our nondimensionalization is different from theirs, a quantitative comparison of the results was not possible.

In Figs. 10 and 11 we show the velocity and temperature distributions for

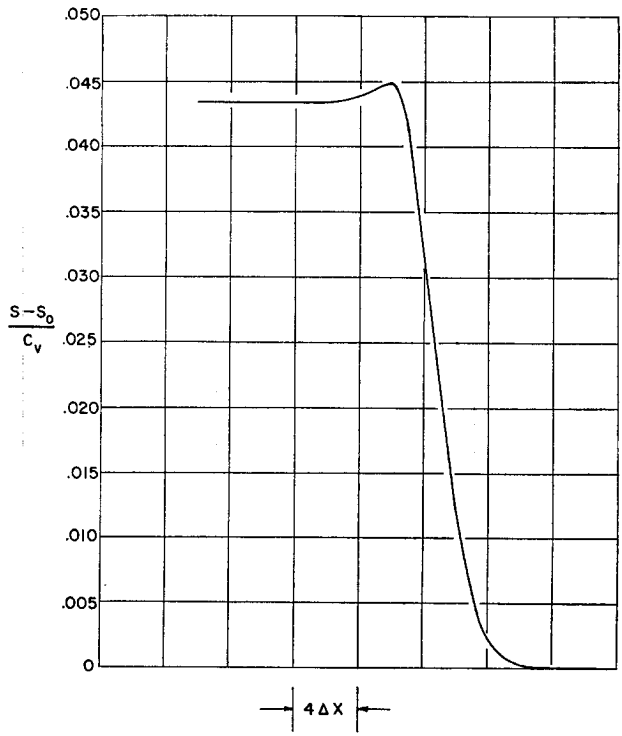

FIG. 12. Entropy distribution for Pr $= \infty$, $Re = 4.5$, $M = 1.6$, $\gamma = 1.4$.

a Prandtl number of $\frac{3}{4}$ and a Reynolds number of 4.5. The shape of the curves remains virtually unchanged for all values of Pr greater than $\frac{3}{4}$.

Figure 12 shows the entropy distribution in the absence of heat conduction but in the presence of viscosity. The Prandtl number is infinite and the Reynolds number is 4.5. The entropy increases monotonically through the shock as a result of viscous dissipation in the absence of conduction.

For finite Prandtl number (Fig. 13) the entropy has a maximum because the time rate of heat loss from the fluid due to conduction near the tail of the shock exceeds the rate at which heat is gained by viscous dissipation.

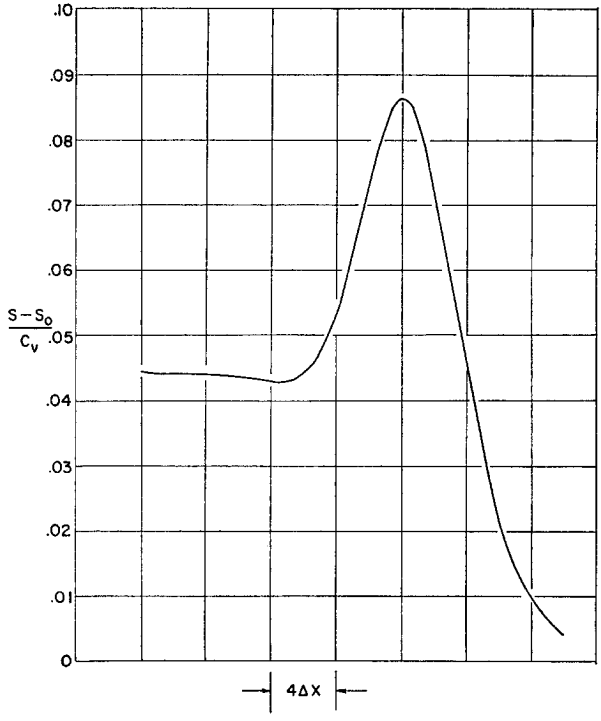

FIG. 13. Entropy distribution for Pr = .75, Re = 4.5, M = 1.6, γ = 1.4.

The last case considered was that of heat conduction without viscosity (Pr = 0). The exact solution for the steady state problem is known; the temperature and velocity rise continuously to a maximum value and then remain constant, whereas the entropy rises to a maximum value and then decreases discontinuously to a lower value; i.e., an isothermal discontinuity occurs.

Our results for this case are shown in Figs. 14–16. The oscillations behind the shock are numerical.

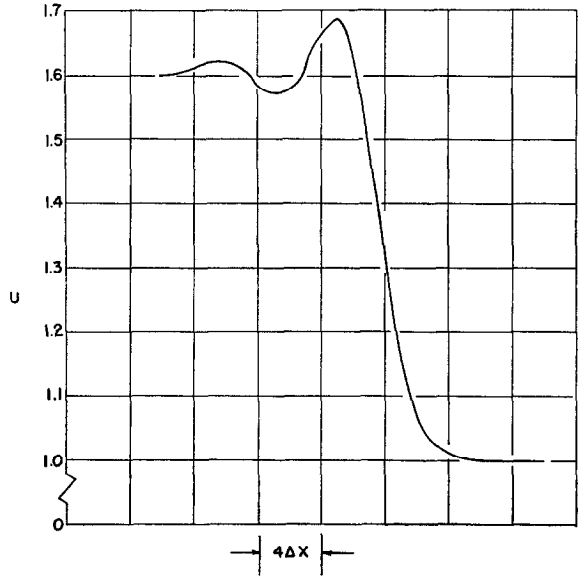

FIG. 14. Velocity distribution for Pr = 0, $M = 1.6$, $\gamma = 1.4$.

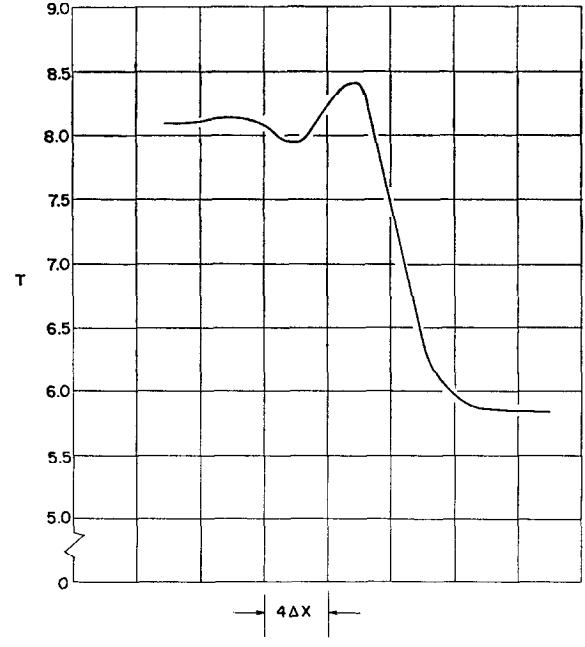

FIG. 15. Temperature distribution for Pr = 0, $M = 1.6$, $\gamma = 1.4$.

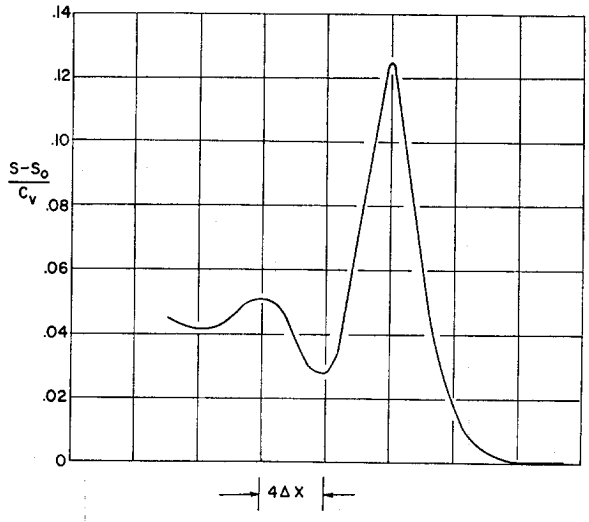

FIG. 16. Entropy distribution for Pr = 0, $M = 1.6$, $\gamma = 1.4$.

REFERENCES

1. R. D. RICHTMYER, "A Survey of Difference Methods for Non-Steady Fluid Dynamics," National Center for Atmospheric Research, Technical Note 63–2 (1963).
2. S. Z. BURSTEIN, *J. Computational Phys.* **1**, 198–222, (1966).
3. D. HOUGHTON, Private communication; June (1966).
4. J. VON NEUMANN, "Progress Report on the Theory of Shock Waves," National Defense Research Committee Division 8, Office of Scientific Research and Development No. 1140 (1943).
5. P. LAX and B. WENDROFF, *Commun. Pure Appl. Math.*, **13**, 217–237 (1960).
6. H. U. THOMMEN, *Z. Angew. Math. Phys.* **17**, 369 (1966).
7. J. GARY, "Some Implicit Finite Difference Schemes for Hyperbolic Systems," AEC Research and Development Report, NYO-1, 426, March (1963).
8. M. MORDUCHOW and P. A. LIBBY, *J. Mecan. Phys. Atmosphere* **4**, 191–213, June (1965).